CHARACTERIZATION OF ADHESION AT CARBON FIBER-FLUORINATED EPOXY INTERFACE AND EFFECT OF ENVIRONMENTAL DEGRADATION

By

SUMAN DASGUPTA

Bachelor of Science in Mechanical Engineering
Jadavpur University
Kolkata, West Bengal, India
2009

Submitted to the Faculty of the
Graduate College of
Oklahoma State University
in partial fulfillment of
the requirements for
the Degree of
MASTER OF SCIENCE
June, 2011

CHARACTERIZATION OF ADHESION AT CARBON FIBER-FLUORINATED EPOXY INTERFACE AND EFFECT OF ENVIRONMENTAL DEGRADATION

Thesis Approved:

Dr. Raman P. Singh

Thesis Advisor

Dr. A. Kaan Kalkan

Dr. Kevin Ausman

Dr. Mark Payton

Dean of the Graduate College

ACKNOWLEDGMENTS

It has been a fantastic experience throughout the last two years here at Oklahoma State University and it would have not been possible without the individuals who have been beside me all along the journey. First of all, my heartfelt thanks to my advisor, Dr. Raman Singh, without whom, graduate studies in the United States would remain an unfulfilled dream for me. I consider it my good fortune to have the opportunity to work under him and get to learn such a lot from him these last two years. His support and encouragement made the tough get going when the going got tough. It was exciting to learn from him even outside work environment due to his vast knowledge on diverse topics.

I would like to thank Dr. Kalkan and Dr. Ausman for their precious time and support. Their inputs on this thesis at short notice was really helpful.

I would like to thank Dr. Gajendra Pandey who has been a constant support and an individual who I could turn to, with any question during my research, and he would be there to answer even in the busiest of times. His cheerful and lively presence helped in difficult situations. I would also like to thank Dr. Nawani and Seshumani for their advice in chemistry related topics.

My experience at the Mechanics of Advanced Materials Lab (MAML) would not have been the same without my wonderful lab mates. Arif has been there since day one and working alongside him has been an experience I would cherish in days to come. His hard work and diligence has been exemplary. I took upon this project from Chirag who was my mentor in my early days here. I would like to thank him for all his support. I would also like to thanks Phil (one of my best buddies around),

Austin (soccer, tennis, frisbee, courses... so much more...), Hamim (Fifa, soccer and breaking the language barrier!), Mohammed (Liverpool vs Man Utd...driving in the blizzard!), Sadia (hope you get done soon... best wishes), Chaitanya, Vasudevan and Balaji. Leila and Masoud are the most soft-spoken and helpful persons one can find and I can't thank them enough for helping me out in my research when I needed it most. I would also like to thank Krishna Bastola for helping me out with chemistry related experiments.

Last but not the least, I would like to name three individuals who made me feel home, far away from home. Abhisek Bhadra, Kunal Mishra and Abhishek Jain had been my roommates when I first came to Tulsa. Not all of us still stick around but I am grateful to have been in the company of such wonderful people. They are the best roommates ever. Abhisek-da had been like an elder brother and I thank him for all his support.

Finally, I would like to thank my parents, Amma and all my family members whose love and blessings have always been beside me through thick and thin.

TABLE OF CONTENTS

LIST OF TABLES

LIST OF FIGURES

CHAPTER 1

INTRODUCTION

1.1 Problem Statement

Carbon fiber reinforced polymers (CFRP) are excellent candidates for aerospace, automobile and other mobile applications due to their high specific strength and modulus. The most prominent aerospace application of carbon fiber composites in recent times is the Boeing 787 Dreamliner, which is the world's first major commercial airliner to extensively use composite materials. The 787 has 50% of its weight made of composites and is 20% more fuel efficient than the similar sized Boeing 767 [2]. Another upcoming commercial airliner which comprises similar percentages of CFRP as structural material is the Airbus 350 and it even has 8% less operating cost than the 787. A light combat aircraft, the HAL Tejas has been developed indigenously by India which employs CFRP's for up to 45% of its airframe weight. Figures 1.1 and 1.2 show the material composition in these aircrafts. Other than the lowering of weight of an aircraft, the advantages of using composites as compared to an all-metal design is that there are lesser fasteners involved which reduce the susceptibility to fatigue failures. The critical issue which needs to be addressed hereby is long-term safety. Hence, long-term durability of composite materials in such applications becomes a point of concern.

Conventional polymer matrices, such as thermosetting resins which are used as the matrix material in carbon fiber composites are susceptible to degradation in the form of chemical corrosion, UV degradation and moisture, in severe environmental conditions. Matrix-influenced properties such as transverse strength and modulus, in-

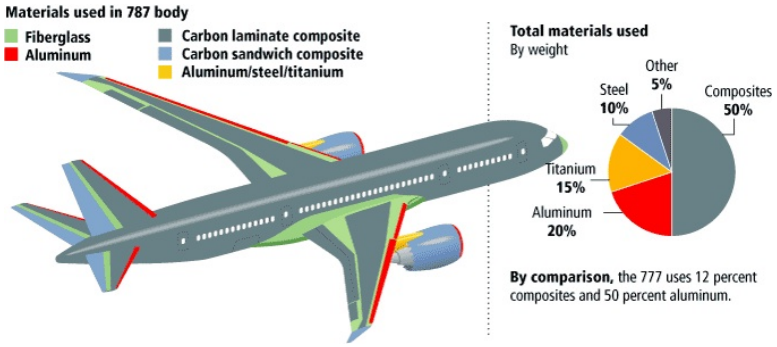

Figure 1.1: Boeing 787 material composition [2].

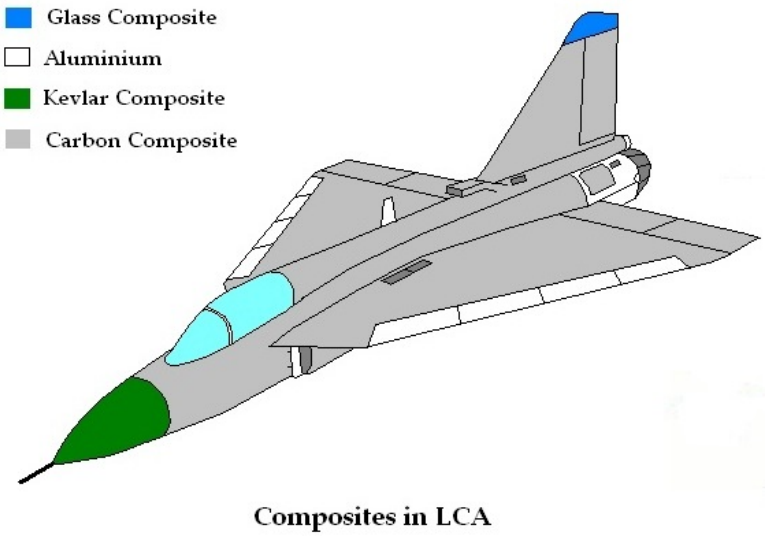

Figure 1.2: Tejas material composition [3].

plane shear strength, and inter-laminar shear strength are deteriorated by degradation of the polymer matrix. In addition, the fibers and the fiber-matrix interphase are also affected. Understanding the degradation mechanisms at the interphase is of vital importance since the interface governs the load transfer from the fiber to the matrix and vice versa. If the fiber-matrix interaction is weak, the composite performance deteriorates. Hence the need for high performance composites with good interfacial characteristics, which can withstand hostile application environments.

Fluorinated polymers offer a viable option as matrix material due to their ability to withstand high temperatures and chemical corrosion, moisture resistance and resistance to UV degradation. They are prepared by reacting one or more fluorinated groups with epoxide groups. Since these polymers are not much susceptible to Van der Waals forces, they are hydrophobic in nature. Also, C-F bonds are significantly stronger than C-H bonds. Moreover, the polymer chains orient themselves in a way such that the fluorine atoms, which are much larger than hydrogen atoms, form a protective envelope for the relatively weak C-C bonds [10]. All these properties suggest that fluorinated polymers can be used to fabricate high performance composite materials, which are expected to show strong inertness to environmental degradation. But it remains to be seen whether the interaction of fluorinated polymers with carbon fibers is strong enough to ensure effective load transfer at the fiber-matrix interface.

The fluorinated epoxy system studied in this project was developed by scientists at the NASA Langley Research Center. Previous projects in our research group have characterized the adhesion at the interface of this epoxy and carbon fibers through the microbond test [1]. In the microbond test, a single epoxy droplet was sheared away from a single carbon fiber, and the force at which de-bonding of the epoxy droplet starts, was measured. The average Interfacial Shear Stress (IFSS) was calculated by dividing this de-bonding force by the area of the fiber-matrix droplet interface. The IFSS data distribution was not symmetrical about the mean. So, a Weibull analysis

was used to analyze the data rather than a normal distribution or similar functions. The Weibull probability distribution function is given by:

$$P_f = 1 - \exp[-(\sigma/\sigma_\theta)^m]\sigma > 0$$

Where P_f is the probability of failure, σ_θ is the Weibull characteristic strength, and m is the Weibull modulus.

The results obtained after the Weibull analysis of interfacial shear strength data of the two microcomposite systems are summarized in Table 1.1. The interfacial shear strength of the fluorinated epoxy based carbon fiber composites was higher than that of the nonfluorinated epoxy based carbon fiber composites before moisture degradation. After aging of the samples using boiling water degradation, there was a 43% reduction in the IFSS of fluorinated epoxy based microcomposites compared to only a 9.2% decrease in the IFSS of non–fluorinated epoxy based microcomposites. This showed that the fluorinated epoxy based microcomposites were degraded more than their non–fluorinated epoxy counterparts. Nonetheless, fluorinated epoxies, due to their hydrophobic nature, are expected to show greater resistance to moisture absorption. The objective of this research is to examine this anomaly.

Fiber	**Matrix**	**Degradation**	**IFSS (MPa)**	**Weibull Modulus**
IM7	DDS-TGMDA	None (As received)	88.7	3.2
IM7	6F-TGMDA	None (As received)	94.8	3.2
IM7	DDS-TGMDA	BWD for 48h	80.5	5.5
IM7	6F-TGMDA	BWD for 48h	53.5	5.0

Table 1.1: Experimental results for fluorinated and non–fluorinated epoxy carbon fiber composite systems before and after boiling water degradation [1]

Pisanova *et al.* [11] showed that the Interfacial Shear Stress method to characterize interfacial adhesion had its inherent drawbacks. It assumes a perfect interface between

the fiber and the matrix and calculates average IFSS over the entire embedded length of the droplet. Also, it does not account for pre-existing stresses at the interface which arise during the curing process. These stresses can occur due to differences in coefficients of thermal expansion(CTE) and Poisson's ratios of the fiber and matrix. Moreover, to characterize adhesion between two surfaces, which is a phenomenon governed by normal surface forces, calculating the normal stresses is a more accurate analysis than average interfacial shear stress. Piggott *et al.* [12] showed that crack initiation in the microbond test and other pull out tests occured in Mode I, that is, normal stresses were involved. Scheer and Nairn [4] showed that the shear stress was zero at the point where the fiber enters the matrix while the normal stresses were maximum at that location, as seen in Figure 1.3. Hence it was very important to calculate normal pressure at the point of debonding rather than the shear stress and thus relate this normal pressure to the work of adhesion.

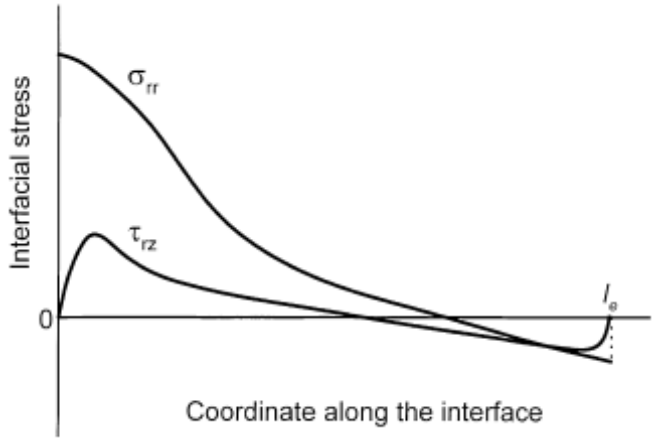

Figure 1.3: Radial, σ_{rr}, and shear, τ_{rz}, interfacial stress distribution along the embedded length in the microbond test [4].

Some of the techniques typically used by researchers to estimate the work of adhesion between two solids are wetting [13–15] and inverse gas chromatography [16]. But these too, are not suitable for measuring fiber-matrix adhesion because of the following disadvantages:

• They calculate the reversible work of adhesion, where two surfaces can be detached if the same amount of energy is supplied to the interface as was released in creating it. The process of fiber-matrix interface formation is irreversible since during curing of the epoxy, there is cross-linking and opening of epoxy rings.

• These processes ignore possible chemical bonding between the fiber surface and the epoxy.

• Finally, the conditions of manufacturing of the composite and testing of adhesion affect the work of adhesion calculation which is not accounted for.

Pisanova *et al.* [11] correctly related the results from destructive micro-mechanical tests such as the microbond test and the single fiber pull out test to calculate the interfacial adhesion. The focus of this study is to determine the adhesion at the carbon fiber-fluorinated epoxy interface using the approach proposed by Pisanova *et al.* and also determine the effect of environmental degradation on the adhesion for the two different matrix systems.

1.2 Fluorinated Epoxy Resins

The principal reason behind using fluorinated resins as matrix materials for composite structures is their reduced susceptibility to environmental degradation. Researchers have postulated novel resin compositions which incorporate fluorine in the monomer in order to utilize the hydrophobicity of the fluorine atom and the more stable C–F bonds. Tao *et al.* [17] synthesized a novel fluorinated resin which showed improved dielectric properties over the commercially available diglycidyl ether of bisphenol A (DGEB-A) due to low polarizability of the C–F bond and large free volume of the CF_3 groups. This resin also showed reduced moisture absorption. Sasaki *et al.* [18] reported that perfluorobutenyloxyphthalic anhydride cured bisphenol A type epoxy could reduce the water absorption by 75%. Hayward *et al.* [19] studied the moisture

absorption in halogenated resin systems and found that there is a lower percentage of bound water in fluorinated resins. Two independent studies by Chong *et al.* [20] and Ho *et al.* [10] showed that fluorination of carbon fiber surfaces improved wetting and adhesion characteristics of the fiber to the epoxy as compared to oxidation. All these studies point to the increased environmental durability of fluorinated resins, especially in the presence of moisture. Also, it can be seen that although studies have been ongoing regarding the characterization of fluorinated resins independently, not much work has been done to characterize the fluorinated resin–carbon fiber interface. Also, the resin system studied in this project is unique since it has been developed quite recently by polymer scientists at the NASA Langley Research Center. Most importantly, the approach which has been adopted in this study to characterize the interface incorporates a number of factors which are usually overlooked in other adhesion characterization methods.

1.3 Interfacial Adhesion from Micromechanical Tests: The concept of adhesional pressure

Micromechanical tests have been utilised to characterize the fiber-matrix interface of fiber reinforced polymer matrix composites since long. The single fiber pull-out test has been employed by many researchers to determine adhesion at the carbon fiber-epoxy interface [21–26]. Another popular method for interfacial characterization is the single fiber fragmentation test (SFFT). Deng *et al.* [27] studied the fiber fragmentation process in several carbon fiber–epoxy composite systems. Schutte *et al.* [28] used SFFT to characterize the effect of moisture degradation on glass fiber–epoxy interfaces. Some other researchers used the SFFT for high strain rates and for interfacial toughness characterization [29–31] and even in most recent studies, this test was used to study the interface of natural fibre–polypropylene composites [32]. Miller *et al.* [33] first used the microbond technique to characterize the fiber–matrix

interface which was later followed by a number of other researchers [34–42].

Comparisons between the several micromechanical test methods were done by HerreraFranco and Drzal [43, 44] and it was postulated that assumption of uniform interfacial shear stress along the embedded length of the fiber led to inaccuracies in the characterization of the interface through these tests. Zhandarov *et al.* [45] proposed a new criterion for interfacial failure, adhesional pressure, which could be determined from the microbond test. This idea was carried further by Pisanova *et al.* [11] who estimated the real level of adhesion in a particular fiber–matrix interphase in terms of the work of adhesion. This analysis introduces a stress-based criterion for interfacial failure wherein the critical normal stress at the fiber–matrix interface is considered to be the failure parameter. This critical normal pressure at the interface is termed as adhesional pressure, σ_{ult}. Scheer and Nairn [4] used a variational mechanics analysis to design an algorithm which calculates the adhesional pressure from the microbond test. The important parameters in this analysis are the material properties of the fiber and matrix, the embedded length of the fiber in the matrix droplet and the debond force when the matrix droplet starts debonding from the fiber. The following parameters are required to be known to calculate the adhesional pressure:

Fiber Properties

Fiber Radius, r_f, Axial Tensile Modulus, E_A, Transverse Modulus, E_t, Axial Poisson's Ratio, ν_A, Transverse Poisson's Ratio, ν_t, Axial Shear Modulus, G_A, Axial CTE, α_A, Transverse CTE, α_t, Embedded Length, l_e.

Matrix Properties

External Radius of Specimen, R_m, Tensile Modulus, E_m, Poisson's Ratio, ν_m, Shear Modulus, G_m, CTE, α_m.

Volume fractions of the fiber and the matrix are determined as:

$$V_f = \left[\frac{r_f^2}{R_m^2}\right] \tag{1.1}$$

$$V_m = 1 - V_f \tag{1.2}$$

Thus, the stress applied to the droplet when the crack initiates is calculated as:

$$\sigma_m = \left[\frac{F_d}{\pi r_f^2}\frac{V_f}{V_m}\right] \tag{1.3}$$

A number of auxiliary constants depending on sample geometry and mechanical and physical properties of the fiber and matrix are calculated (Appendix A). A dimensionless co-ordinate system is defined along the specimen geometry of the microbond specimen as shown in Figure 1.4. Functions $\phi(\zeta)$ and $\psi(\zeta)$ are defined in terms of the dimensionless co-ordinate along the embedded length, ζ, as follows:

$$\phi(\zeta) = \left(\psi_0 + \frac{\sigma_m V_m}{2V_f}\right)\phi_e(\zeta) + \frac{\sigma_m V_m}{2V_f}\phi_o(\zeta) \tag{1.4}$$

$$\psi(\zeta) = \psi_0 - \phi(\zeta) \tag{1.5}$$

where $\psi_0 = -\frac{D_3 \Delta T}{C_{33}}$ and $\phi_e(\zeta)$ and $\phi_o(\zeta)$ are even and odd hyperbolic functions of ζ.

Adhesional pressure, σ_{ult} was calculated at the point where the fiber entered the matrix ($\xi = 1, \zeta = \rho$) as shown in Figure **??** according to the following equation:

$$\sigma_{ult} = \sigma_{rr,f}\,|_{\zeta=\rho}^{\xi=1} = \frac{\ddot{\psi}(\zeta)\,|_{\zeta=\rho}}{16}\left[3 + \nu_m + \frac{2(1+\nu_m)lnV_f}{V_m} - \frac{V_m A_1}{V_f A_0}\right] - \frac{V_m}{V_f}\left[\frac{A_3\psi(\rho) + A_5\Delta T}{A_0}\right] \tag{1.6}$$

Having obtained the adhesional pressure or ultimate normal stress at the interface, the Work of Adhesion is obtained from an empirical relation developed by Pisanova

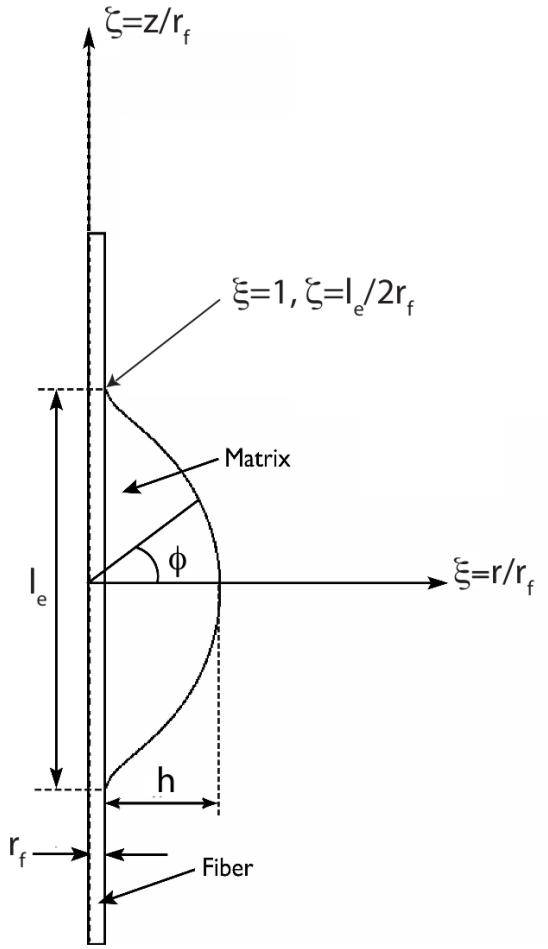

Figure 1.4: Dimensionless co-ordinate system used to analyze the microbond specimen (half of the cross-section geometry shown)

et al [11] as per:

$$W_A = 64 + 0.32(\sigma_{ult} - 82) mJ/m^2 \tag{1.7}$$

where, σ_{ult} is the adhesional pressure in MPa.

In this study, we look to determine the work of adhesion at the interface of IM7 carbon fiber–fluorinated epoxy and monitor the effect of moisture degradation on the work of adhesion. Also, the adhesional pressure values obtained are compared with the interfacial shear stress obtained from previous projects to determine the validity of this approach.

CHAPTER 2

MATERIALS

The resin systems used in this study were supplied by Dr. Jeffrey Hinkley (NASA Langley Research Center, Hampton, VA). They included a fluorinated epoxy and a non-fluorinated epoxy based on tetraglycidyl methylene dianiline (TGMDA). The goal was to characterize the interfacial adhesion from the microbond test, where single droplets of these epoxies were deposited on single carbon fiber filaments. The fibers used in the study were single filament, unsized HexTow IM7 carbon fibers (Hexcel Corporation, Stanford, CA) [46].

The principal epoxy, TGMDA is a tetrafunctional epoxy which is a major component of high performance matrix systems used for advanced aerospace grade composites. Figure 2.1 shows the chemical structure of tetraglycidyl methylene dianiline epoxy. These epoxies are characterized by high cross-linking densities which results in high modulus of elasticity and high glass transition temperature. However, the high crosslink densities of these epoxies are also accompanied with low strain to failure values and high moisture absorption levels [5].

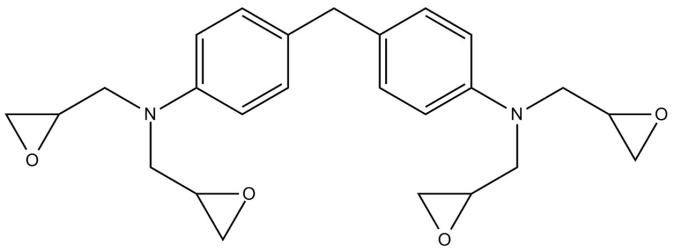

Figure 2.1: Chemical structure of tetraglycidyl methylene dianiline [5]

Diamino diphenyl sulfone (DDS) is the curing agent used with the TGMDA epoxy

resin to form the non-fluorinated resin. DDS when used with TGMDA results in superior thermal stability and mechanical properties such as tensile, flexural and glass transition temperatures [6]. Figure 2.2 shows the chemical structure of diamino diphenyl sulfone.

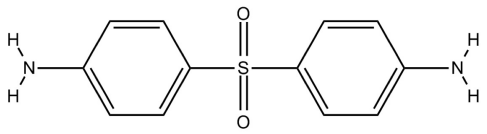

Figure 2.2: Chemical structure of DDS [6].

6F-diamines or 2,2 bis(4-aminophenyl) hexafluoro propane is a fluoropolymer polyimide which when blended with TGMDA forms the fluorinated epoxy studied in this project. The chemical structure of the resultant fluorinated epoxy, 4,4-methylene bis-[N,N-bis(2,3-epoxy propyl)-3-trifluoromethylaniline] which is referred to as 6F TGMDA henceforth, is shown in Figure [8]. Based on the research done at NASA Langley Research Center, these fluorinated epoxies show greatly reduced moisture absorption as compared to the conventional DDS-TGMDA based epoxies [7]. Due to their low moisture uptake characteristics, these fluorinated epoxies could be used as a matrix or as a fiber surface coating in a composite which would therefore potentially result in improved long term durability against environmental effects. However, it remains to be checked if these epoxies have mechanical properties suitable for use in fiber reinforced composites.

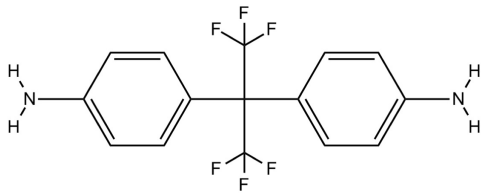

Figure 2.3: Chemical structure of 2,2 bis(4-aminophenyl) hexafluoro propane [7].

In this study, the coefficient of thermal expansion (CTE) of 6F TGMDA and DDS TGMDA were determined using a curvature measurement technique, Coherent

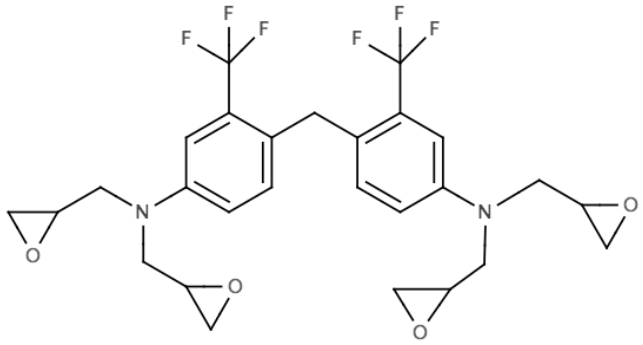

Figure 2.4: Chemical structure of 6F TGMDA [8].

Gradient Sensing (CGS). This technique is relatively new and the sample preparation methods were not as per any give standards. Hence, the results obtained needed to be verified with available literature. So, first of all, trial runs of the experiment were performed using an epoxy of known CTE, EPON 862® (Hexion Speciality Chemicals, Columbus, OH) which is a diglycidyl ether of bisphenol F based resin. The curing agent used for this epoxy was Epikure 3274® (Hexion Speciality Chemicals, Columbus, OH), a low viscosity aliphatic amine. Both materials were purchased from Miller Stephenson Chemical Company (Tulsa, OK). The chemical structures of EPON 862® and Epikure 3274® are shown in Figures 2.5 and 2.6.

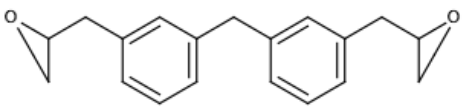

Figure 2.5: Chemical structure of Diglycidyl ether of bisphenol F (EPON 862®) [9].

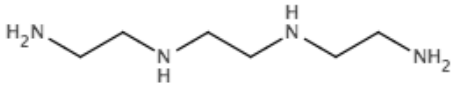

Figure 2.6: Chemical structure of aliphatic amine curing agent, Epikure 3274®

[9]

Also, the mold required for holding nano-indentation samples were prepared from

Epofix resin (Bisphenol-A, epichlorhydrin) mixed with 12.5 wt % Epofix hardener (Triethylenetetramine and 2-(2-Aminoethylamino) ethanol) obtained from Struers A/S, Denmark.

CHAPTER 3

EXPERIMENTS

There were two properties of the non-fluorinated and fluorinated epoxies that were to be determined, namely the elastic modulus and coefficient of thermal expansion. These were required to calculate the adhesional pressure at the interface, from where the work of adhesion would be estimated.

3.1 Determination of Young's Modulus

The epoxies were available in very small amounts, around 2 grams of each. So, samples were made either in the form of thin films or small sized globules for nanoindentation. Two methods were employed to determine the elastic modulus of the epoxy: (i) three point bend tests on composite beams prepared by depositing thin films of the epoxy on 22 mm×22 mm glass cover slips and (ii) nano-indentation.

3.1.1 Three-point bend tests on thin epoxy films

First, trial experiments were done with EPON 862 films to validate the approach since the sample preparation method for the three point bend tests were not according to any ASTM standard due to very small amounts of the epoxy available. A glass slide was taken and a coating of chemical release agents was applied on it. Then, a droplet of EPON 862, cured with Epikure 3274 was deposited on the slide and a 22 mm×22 mm glass cover slip used to smear the droplet so as to make a uniform thin film. Figure 3.1 shows the sample preparation method.

With the cover slip still in place, the set up was cured at room temperature for

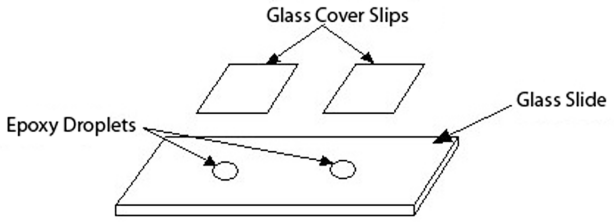

Figure 3.1: Sample preparation for three point bend tests on thin films

24 hours and then post cured at 121°C for 6 hours. Then the cover slip with the film on it was detached from the base slide using a razor blade. The resulting sample resembled a composite beam of glass and epoxy. Three point bend test was done on these samples on a universal testing machine (Instron 5567, Norwood, MA) to determine the flexural modulus of EPON 862. The three point bend test gave the effective modulus of the composite beam and with the modulus of glass known, the epoxy film modulus could be calculated from the following equation:

$$E_{eff} = \frac{E_g E_f (t_g + t_f)}{E_g t_g + E_f t_f} \tag{3.1}$$

The values of flexural modulus obtained from these experiments were found to be in the same range as the ones obtained by bulk sample testing of EPON 862. Hence, these were repeated for the fluorinated and non-fluorinated epoxies. However, the effect of boiling water degradation (BWD) on the modulus of these epoxies were also to be determined. When these composite beams were subjected to BWD for 24 hours, the epoxy films started to peel off from the glass cover slips as seen in Figures 3.2(a) and 3.2(b). Hence they could not be tested post-degradation. So, nanoindentation methods were resorted to determine the glassy modulus of the epoxies before and after moisture degradation.

3.1.2 Nanoindentation

The samples for nanoindentation were prepared by depositing a small amount of the epoxy in an Epofix mold. The Epofix mold was made by mixing Epofix resin with

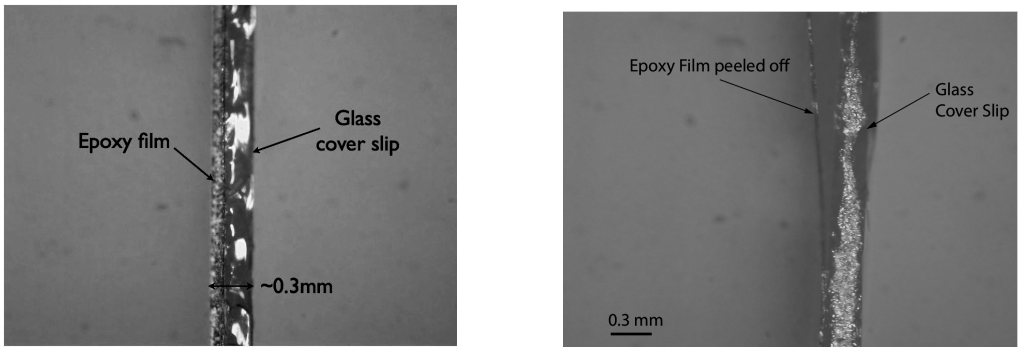

(a) Film before BWD (b) Film after BWD

Figure 3.2: Side view of the DDS TGMDA-Glass composite beam before and after BWD

12.5 wt % Epofix hardener and casting them in cylindrical casings of 1 inch diameter. The molds were cured for 24 hours at room temperature. For convenience, each cylindrical mold was cut into four quarters to increase the number of samples which could be made from a single Epofix mold. Then, small holes of 1/16th inch diameter were drilled into the center of each quarter as shown in Figure 3.3.

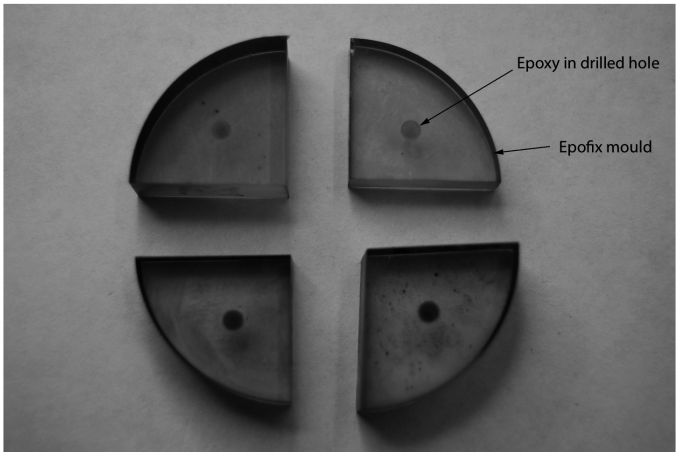

Figure 3.3: Sample preparation for Nano-indentation

The fluorinated and non-fluorinated epoxies were carefully deposited in the holes while keeping the molds on a hot plate at around 80°C since these epoxies were highly viscous at room temperature. The molds, with the epoxy embedded in them were cured at 177°C for 3 hours, which is the curing cycle used to cure the fluorinated and

non-fluorinated epoxies.

The cured samples were then polished on an Ecomet 3 Variable Speed Grinder Polisher (Buehler, Germany) with 3μm, 1μm, 0.5μm and diamond polishing disks. A batch of 5 samples were nanoindented using Asylum Research MFP 3D Atomic Force Microscope (AFM), by replacing the AFM head with the nanoindenter head. Lu *et al.* proposed a method to calculate Young's relaxation modulus of viscoelastic materials such as polymers, using nanoindentation [47]. Creep and stress relaxation are important time-dependent parameters to characterize viscoelastic materials. Creep is the measure of increase in deformation that occurs under a constant load, in addition to the initial deformation. Stress relaxation is the decrease in stress with time after stressing to a constant deformation, as in the case of loosening of bolts after they are tightened to a certain stress when put into service. According to Lu *et al.*, the relaxation function for a viscoelastic polymer, $E(t)$, could be determined from the loading curve of a constant displacement rate indentation test [47]. The value of the function for $t = 0$ gives the glassy modulus or relaxation modulus for the viscoelastic material which also represents its Young's modulus. The relaxation function can be found from the following equation:

$$E(t) = \frac{\pi(1-\nu^2)\tan\alpha}{4}\frac{d^2P(t)}{dh^2} \tag{3.2}$$

A quadratic function, $P(t)$, is fit into the loading section of the load-displacement plots and the relaxation modulus calculated from the above equation. A Berkovich tip was used because of its well-defined geometry which ensures a more precise control over the indentation process. Constant displacement rates of 0.033, 0.05, 0.067, 0.1 and 0.133 μm/sec were used to load the specimens.

3.2 Determination of Coefficient of Thermal Expansion

The determination of the coefficient of thermal expansion of the epoxy is important since differences in coefficient of thermal expansion (CTE) of the epoxy and the carbon fiber result in thermal stresses at the interphase during curing of the microbond specimen. A unique experimental technique, Coherent Gradient Sensing (CGS) developed by Tippur *et al.* [48], was used to determine the CTE.

3.2.1 Coherent Gradient Sensing

This is a full-field curvature measurement technique which measures gradients of surfaces (CGS in reflection mode), thickness, and refractive indices (CGS in transmission mode). It was first developed to study deformation fields near quasi-static and dynamically growing cracks. Other interferometric techniques give measurable fringe densities only for elastic deformations and are insufficient at large deformations when fringe densities are high. CGS performs satisfactorily over a wide range of deformations. Also, it is insensitive to rigid body displacements and rotations and hence can be used to study dynamically growing crack tips. Rosakis *et al.* [49] used CGS in thin film characterization to measure curvatures in thin films and micro-mechanical structures.

3.2.2 Principle of Coherent Gradient Sensing

CGS uses the principle of diffraction and interference to create fringe patterns from a curved surface which can be analyzed to measure curvature of the surface. For curvature measurements, CGS is used in reflection mode, where a collimated laser beam is projected onto a reflective surface. The reflected beam is passed through two identical high density Ronchi gratings, with identical pitch, separated by a distance Δ. The doubly diffracted orders from the two gratings are then focussed into clear diffraction spots by a convex lens. An aperture is placed at the focal plane of the lens,

where the diffraction spots are formed, which lets through one of the $\pm$ 1 order fringes. This fringe order is then projected on a film and imaged. The working principle of Coherent gradient sensing in two dimensions is shown in Figure 3.4.

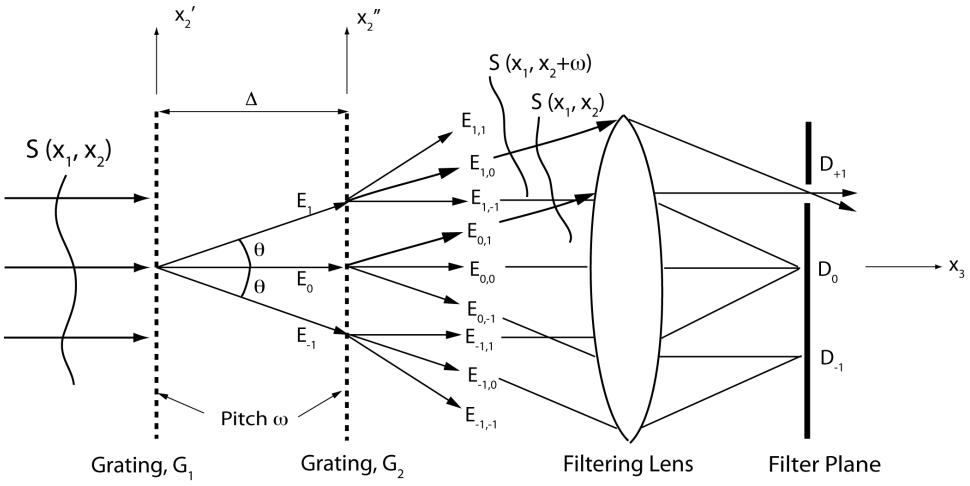

Figure 3.4: The working principle of Coherent Gradient Sensing

As the reflected laser beam from the reflective specimen surface falls on the gratings, let us consider an optical wave front incident on the first grating, G_1. Both gratings have their grating lines running along the X_1 direction such that the wavefront is diffracted along the X_2 direction. After passing through the first grating, the wavefront is diffracted into several wavefronts E_{-1}, E_0 and E_1 as shown in Figure 3.4. Each of these are further diffracted into $E_{1,-1}, E_{1,0}, E_{1,1}, \ldots, E_{0,-1}, E_{0,0}, E_{0,1}$, $\ldots$, $E_{-1,-1}, E_{-1,0}, E_{-1,1}, \ldots$, etc by the second grating, G_2. This gives rise to sets of parallel beams which are converged to distinct diffraction spots using a convex filtering lens. An aperture is placed at the focal plane of the lens which lets through only one diffraction spot, D_{-1} or D_1 to imaged onto a screen behind. The diffracted beams $E_{1,0}$ and $E_{0,1}$ interfere at the focal plane to form the $+1$ diffraction spot. As seen from Figure 3.4, the wavefronts along these beams are shifted by an amount ω and they interfere to form fringe patterns from which curvature of the specimen can be calculated. The ± 1 diffraction spots are also of the maximum intensity and the

intensity decreases as the diffraction order increases. The lateral shift in the wavefronts, ω depends on the distance between the gratings, Δ and the diffraction angle, θ as:

$$\omega = \Delta \tan\theta \tag{3.3}$$

where diffraction angle θ is given by $\theta = \arcsin(\lambda/p)$, λ being the wavelength of the laser beam, and p being the pitch of the grating.

The specimen curvatures along X_1 and X_2, κ_{11} and κ_{22}, can be calculated using a Matlab code which is principally based on the following partial differential equation:

$$\kappa_{\alpha\beta}(x_1, x_2) \approx \frac{p}{2\Delta}\left(\frac{\partial n^{(\alpha)}(x_1, x_2)}{\partial x_\beta}\right), n^{(\alpha)} = 0, \pm 1, \pm 2, \pm 3, \ldots$$

where, p is the pitch of the gratings and Δ is the distance between gratings

The experimental set-up for CGS is shown in Figure 3.5. The He-Ne laser and other optical instruments were obtained from CVI Melles Griot, (Albuquerque, NM) and Newport Corporation (Irvine, CA).

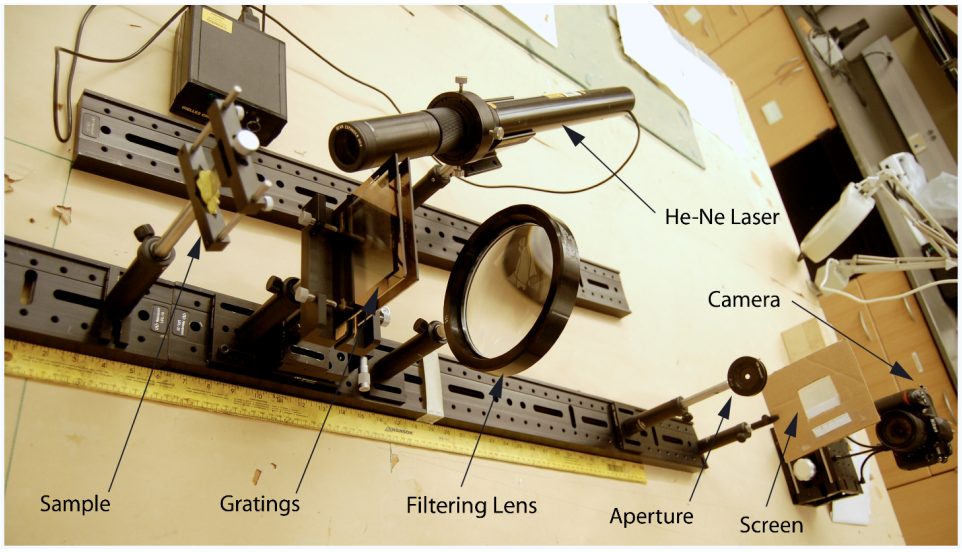

Figure 3.5: Experimental set up for Coherent Gradient Sensing

This concept is utilized here to measure curvature of thin films of the epoxy deposited on glass cover slips. The samples were prepared in similar manner as the

ones prepared for three point bend tests on thin epoxy films, except that one side of the glass cover slips were silver-sputtered to make them reflective, as shown in Figure 3.6.

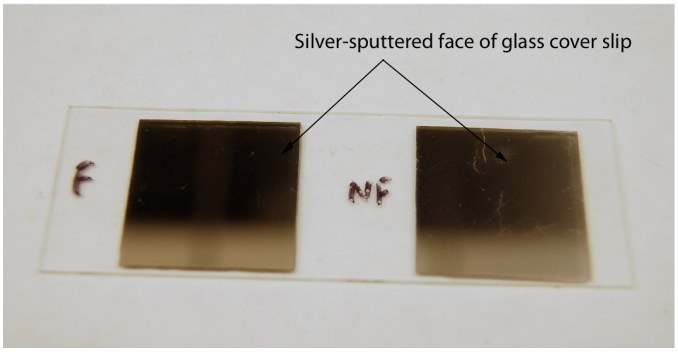

Figure 3.6: Sample preparation for Coherent Gradient Sensing

The samples made were analogous to bimetallic strips comprised of glass and epoxy. Hence, bimetallic strip analysis was used to calculate the coefficient of thermal expansion values of the epoxy from the curvature obtained from CGS. With the volumetric CTE of glass known, the CTE of the epoxy was calculated from the following equation:

$$\kappa = \frac{(\alpha_f - \alpha_g)\Delta T}{\frac{h}{2} + \frac{2(E_f I_f + E_g I_g)}{h}(\frac{1}{E_f t_f} + \frac{1}{E_g t_g})} \tag{3.4}$$

where suffixes g and f represents properties of glass and epoxy film respectively.

When the EPON 862 films were cured at room temperature for 24 hours and then post cured at 121° for 6 hours, there was shrinkage of the epoxy which caused the epoxy-glass composite beams to curve inwards since the epoxy shrank, but glass obviously did not. Now at high temperatures, the cured epoxy would expand more than glass and hence the specimen would tend to curve in an opposite direction to that caused by shrinkage as shown in Figure 3.7. Hence, curvature measurements right after curing proved to be inadequate in correctly measuring CTE since shrinkage played an important role. To overcome this difficulty, the cured samples were re-

heated to 50° and then allowed to cool down to room temperature for them to attain thermal equilibrium. Trial runs were performed with EPON 862, cured with Epikure 3274 and the CTE values obtained agreed closely with those obtained from literature.

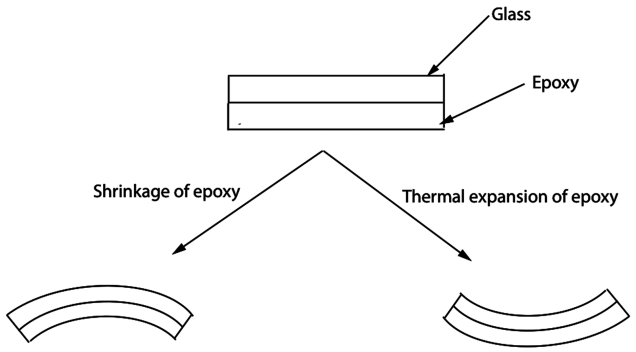

Figure 3.7: Curvature of epoxy film-glass cover slip samples upon curing

CHAPTER 4

RESULTS AND DISCUSSION

4.1 Comparison of Moisture Absorption

The fluorinated and non-fluorinated epoxies were first compared for their moisture absorption characteristics by hourly monitoring the weight gain when they were exposed to moisture at 100% relative humidity at 80°C. Figure 4.1 shows that the non-fluorinated epoxy, DDS TGMDA showed three times higher moisture absorption than the fluorinated epoxy, 6F TGMDA.

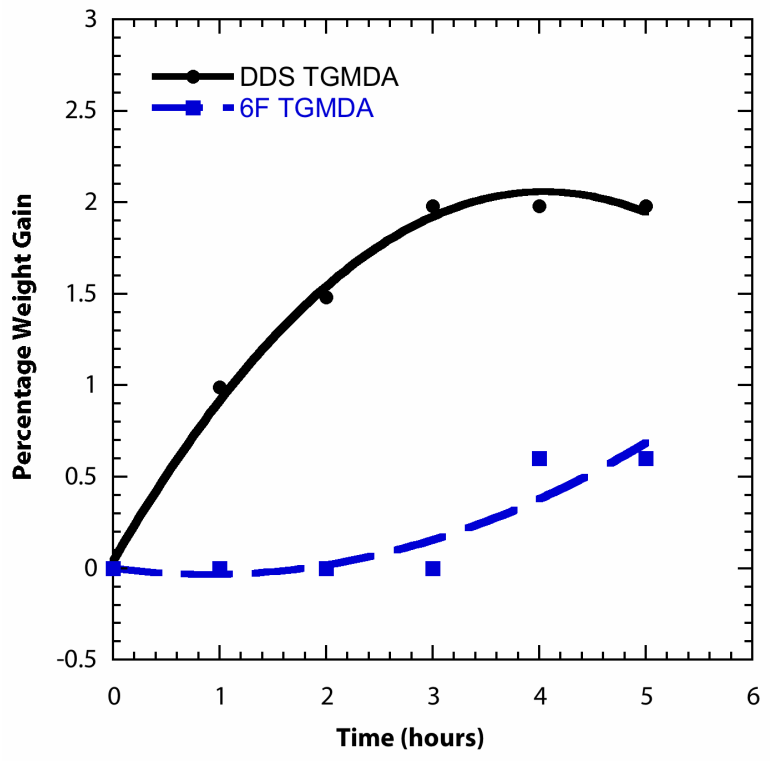

Figure 4.1: Comparison of moisture absorption for 6F TGMDA and DDS TGMDA

The lower moisture absorption rate by the fluorinated epoxy as compared to the

DDS cured epoxy was expected since the higher electronegativity of fluorine makes it hydrophobic in nature. Minute amounts of epoxy samples used to find the moisture absorption rate and hence they saturated within a few hours and the curves hit the plateau region.

4.1.1 Young's Relaxation Modulus: Nanoindentation

A comparison of the load–displacement plots obtained for a particular loading rate of 0.1μm/sec and a load time of 30 seconds are shown in Figures 4.2 and 4.3.

A quadratic function was fit into the loading section of the curves as shown in Figure 4.4. As seen, the fitted curve showed nearly perfect correlation with the nano-indentation load-displacement data.

The indented samples were imaged using Atomic Force Microscopy to see the topography of the indents. Figures 4.5 and 4.6 shows greater depths of indentation and lesser recovery for the moisture degraded samples (6F TGMDA) as compared to the as received ones for identical maximum loads. This further validated the observation from the load-displacement plots that the relaxation modulus was expected to decrease post moisture degradation.

The relaxation modulus values obtained for the two epoxies, 6F TGMDA and DDS TGMDA, before and after Boiling Water Degradation, are summarized in Table 4.1.

4.1.2 Coefficient of Thermal Expansion: Coherent Gradient Sensing

Since the volumetric coefficient of thermal expansion (β) values of the DGEB-F based epoxy, EPON 862®, were known from literature, trial runs were performed with EPON 862® films to ensure that the CTE values obtained were in the same range as expected. The thickness of the silver-sputtered glass cover slips ranged from 190 μm to 200 μm and the EPON 862® film thickness ranged from 39.2 μm to 46.3 μm.

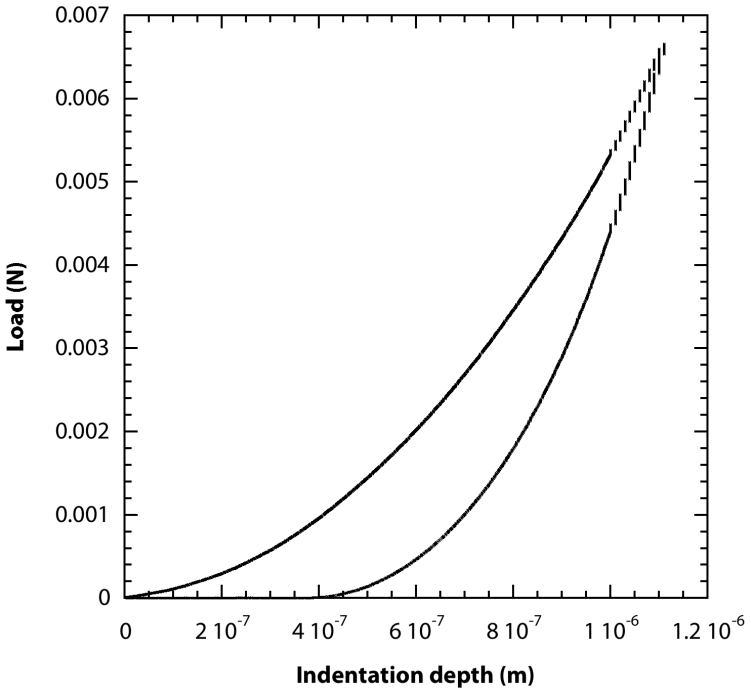

(a) 6F TGMDA as received

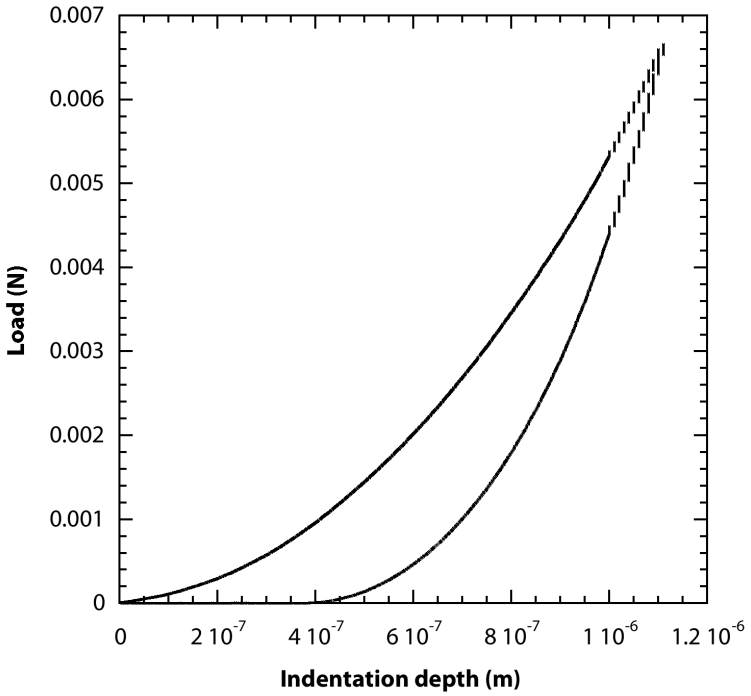

(b) 6F TGMDA post BWD

Figure 4.2: Nano-indentation load–displacement plot for 6F TGMDA (as received and post BWD) at loading rate 0.1μm/sec and loading time 30 seconds

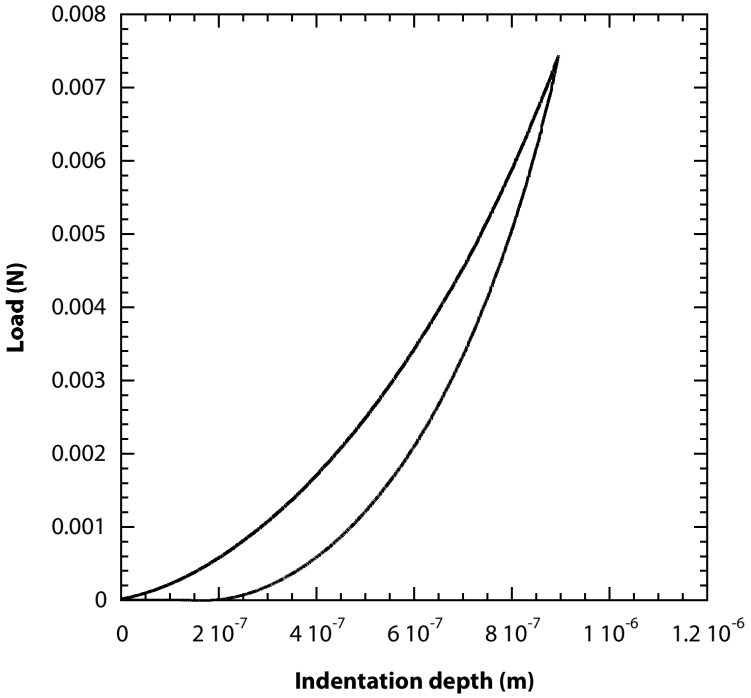

(a) DDS TGMDA as received

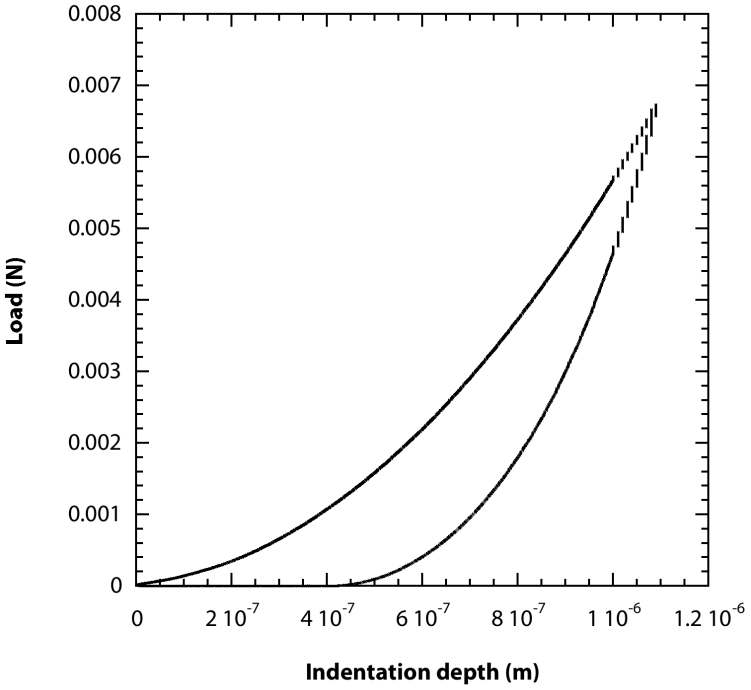

(b) DDS TGMDA post BWD

Figure 4.3: Nano-indentation load–displacement plot for DDS TGMDA (as received and post BWD) at loading rate 0.1μm/sec and loading time 30 seconds

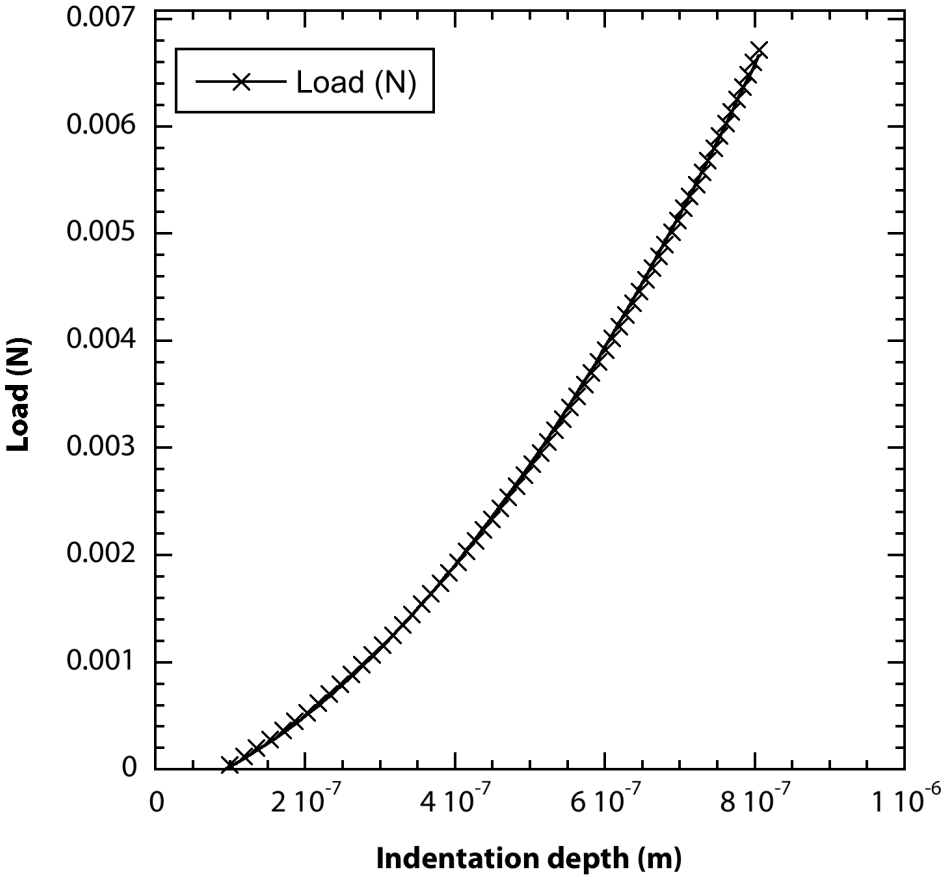

Figure 4.4: Fitted and measured load–displacement curves for 6F TGMDA sample

Matrix	**Degradation**	**Relaxation Modulus (GPa)**
6F-TGMDA	None (As received)	2.89±0.05
DDS-TGMDA	None (As received)	2.71±0.03
6F-TGMDA	BWD for 24h	2.59±0.09
DDS-TGMDA	BWD for 24h	2.58±0.03

Table 4.1: Relaxation Modulus for fluorinated and non–fluorinated epoxies before and after boiling water degradation

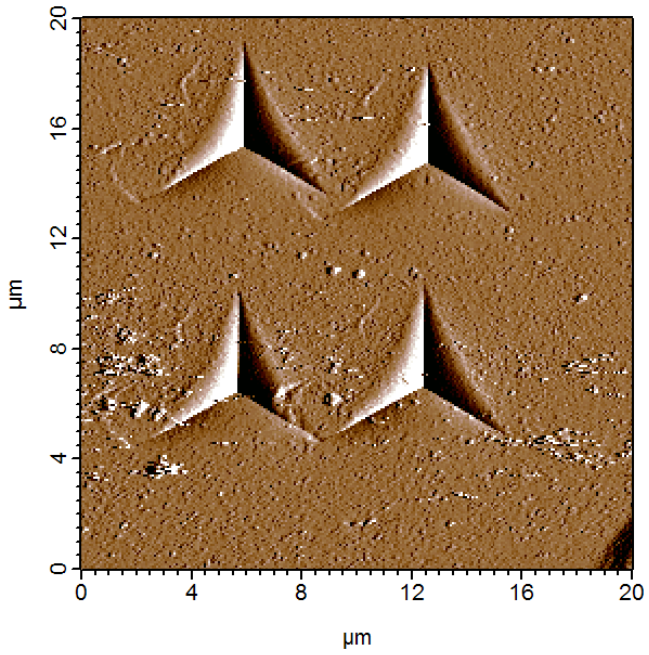

Figure 4.5: AFM image for nano-indented surface of as-received 6F TGMDA sample with loading rate $0.1\mu m/sec$ for 30 seconds

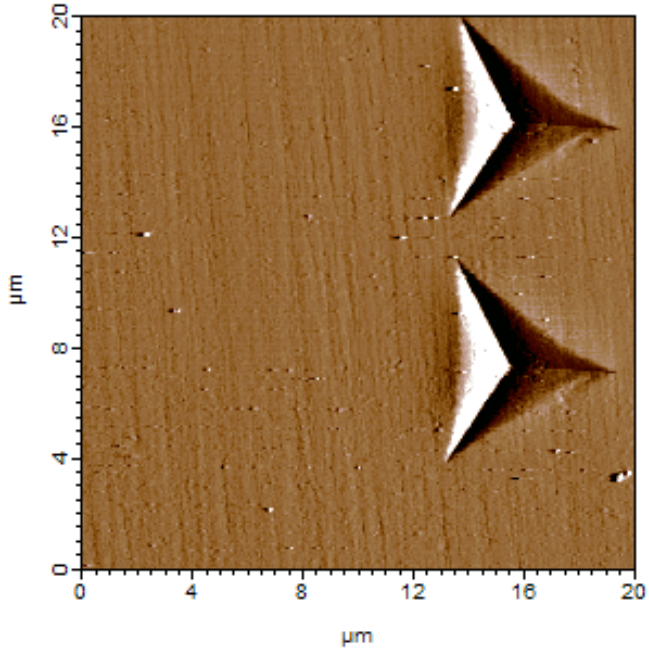

Figure 4.6: AFM image for nano-indented surface of degraded 6F TGMDA sample with loading rate $0.1\mu m/sec$ for 30 seconds

Typical fringe patterns obtained from CGS are shown in Figures 4.7 and 4.8.

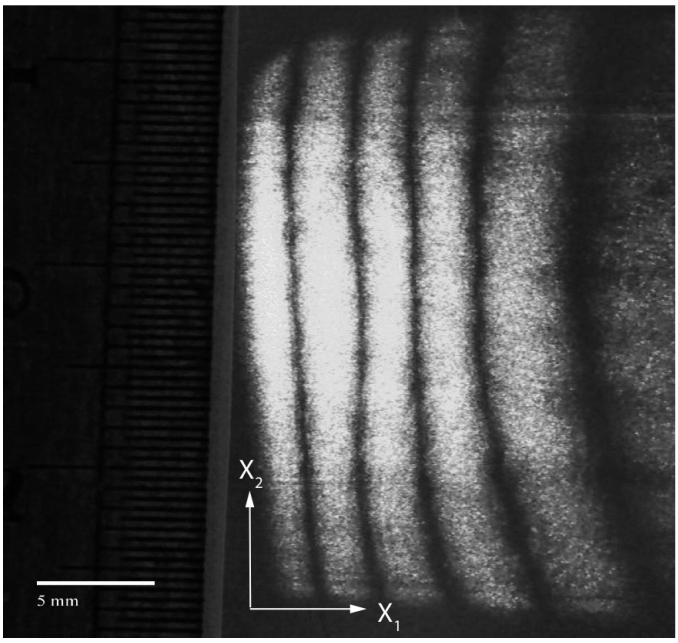

Figure 4.7: Fringe pattern for CGS on EPON 862®: Shearing along X1

While imaging the fringe patterns, a scale was attached adjacent to the screen. This helped in assigning a scale to the image when it was subsequently digitized using a MATLAB program. Using the MATLAB program, an origin was selected on the image. $X1$ and $X2$ co-ordinate axes were defined with reference to the adjacent scale. Then, discrete co-ordinate points were selected on the dark and bright fringes. The points were selected approximately at the center of the width of the individual fringes. Consequent dark and bright fringes were ordered $0, 0.5, 1, 1.5, \ldots$. The first dark fringe was ordered as 0, the next bright fringe 0.5 and so on. It is not of vital importance to order the first dark fringe as 0, which can also be ordered 1 or 2, since only the difference in fringe order of adjacent fringes, which is 0.5, is required to calculate curvature. The output from the MATLAB program contained $X1$ and $X2$ co-ordinate data for all the points selected. The corresponding fringe numbers for each of the points were added to the co-ordinate data. This would serve as the input file to the MATLAB program which calculated curvature of the specimen. An

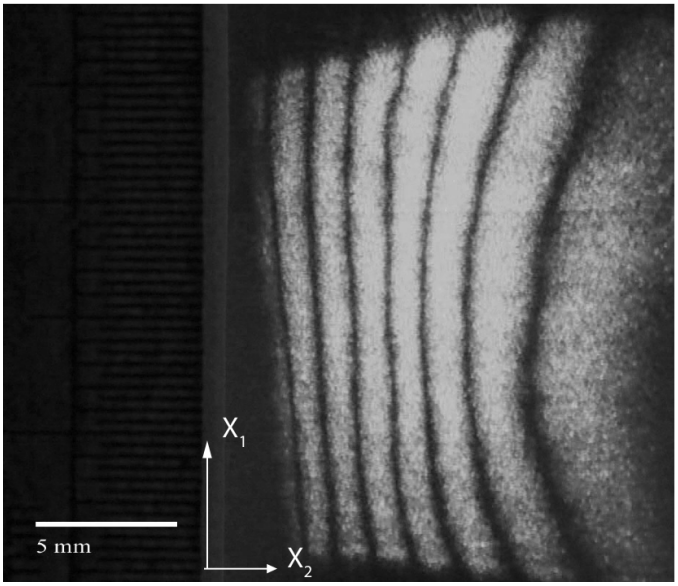

Figure 4.8: Fringe pattern for CGS on EPON 862®: Shearing along X2

example of the co-ordinate points used for fringe digitization is shown in Figure 4.9.

In order to calculate the volumetric CTE of EPON 862®, the CTE of glass was assumed to be 25.5x10^{-6}/°C. The curvature values obtained and the CTE calculated henceforth are shown in Table 4.2.

Shearing axis	**Curvature** (m^{-1})	**CTE (/°C)**	**Average CTE(/°C)**	**Miller *et al* [50](/°C)**
X1	0.38	72.58 x 10^{-6}	85.35±17.03 x 10^{-6}	84±10 x 10^{-6}
X1	0.34	65.26 x 10^{-6}		
X2	0.71	108.29 x 10^{-6}		
X1	0.53	84.74 x 10^{-6}		
X2	0.73	107.92 x 10^{-6}		
X1	0.42	73.61 x 10^{-6}		
X2	0.46	85.08 x 10^{-6}		

Table 4.2: Coefficient of Thermal Expansion for EPON 862® as obtained from CGS

Hence, we can see that the CTE values obtained showed good conformity to the one reported by Miller *et al* at the NASA Glenn Research Center [50]. The greater

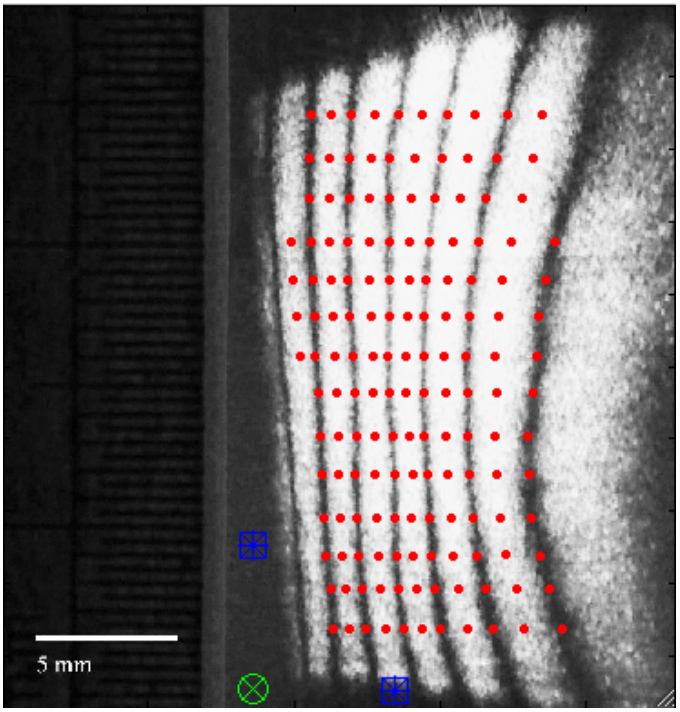

Figure 4.9: Digitization of Fringes: Shearing along X2

amount of deviation is expected due to non-uniformity in thickness of the epoxy film and errors during manually selecting co-ordinate points along the fringe pattern during analysis.

CGS was then performed on 6F TGMDA and DDS TGMDA. One issue faced during these experiments was that the TGMDA based epoxies released air bubbles when heated above room temperature to reduce their viscosity. The films had to be prepared while placing the bottom glass slide on a hot plate and care had to be taken to minimize the number of air bubbles trapped in the film between the glass slide and the cover slip. Typical fringe patterns obtained from the fluorinated and non-fluorinated epoxies are shown in Figures 4.10 and 4.11. The fringe patterns were analyzed after selecting regions where there were no bubbles trapped and uniform fringes were visible. The CTE values calculated for 6F TGMDA and DDS TGMDA are shown in Table 4.3.

The volumetric coefficient of thermal expansion for the fluorinated epoxy is slightly

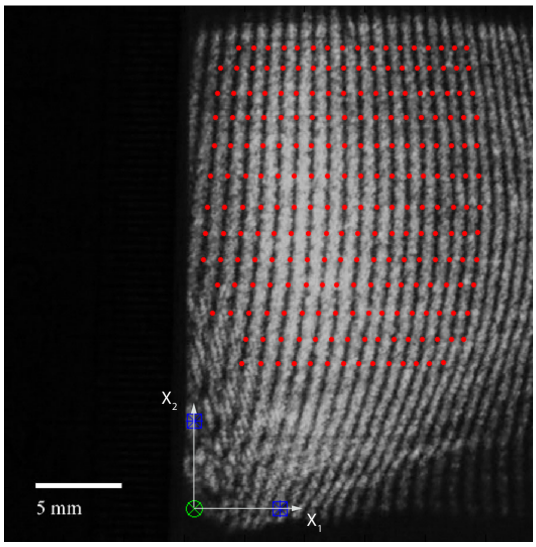

(a) Shearing along X1

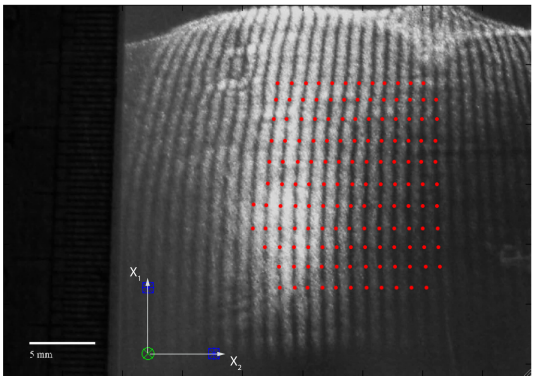

(b) Shearing along X2

Figure 4.10: Fringe pattern for CGS on 6F TGMDA

Epoxy	**CTE (/°C)**
6F TGMDA	35.89±6.25 x 10^{-6}
DDS TGMDA	41.23±6.99 x 10^{-6}

Table 4.3: Coefficient of thermal expansion for 6F TGMDA and DDS TGMDA as obtained from CGS

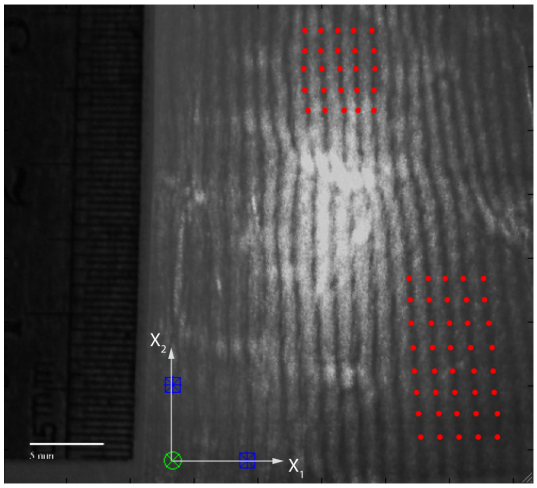

(a) Shearing along X1

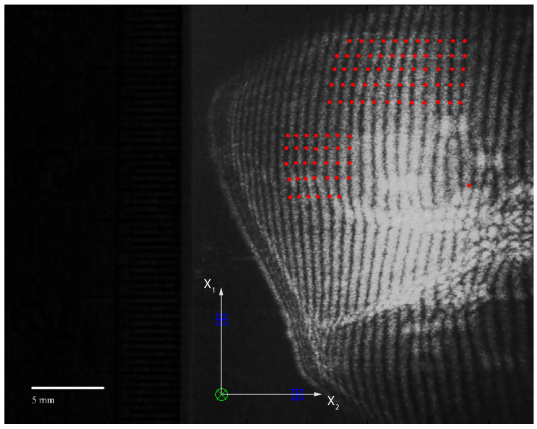

(b) Shearing along X2

Figure 4.11: Fringe pattern for CGS on DDS TGMDA

less than the DDS cured TGMDA resin since the C-F bonds in the fluorinated epoxy are stronger than conventional C-H bonds and thermal expansion decreases with increasing bond energy.

4.1.3 Work of Adhesion

Having obtained the required physical and mechanical properties of the epoxy systems, the work of adhesion at the carbon fiber-epoxy interface was estimated using the analytical approach proposed by Pisanova *et al* [11]. The fiber and matrix properties used in the analysis are shown in Tables 4.4 and 4.5.

Property	**Value**	**Source**
Fiber radius, r_f	5.2 μm	HexTow [46]
Axial tensile modulus, E_A	276 GPa	HexTow [46]
Transverse modulus, E_t	8 GPa	Miyagawa *et al* [51]
Axial Poisson's ratio, ν_A	0.2	Pisanova *et al* [11]
Transverse Poisson's ratio, ν_t	0.3	Miyagawa *et al* [51]
Axial shear modulus, G_A	115 GPa	HexTow [46]
Axial CTE, α_A	-0.4 x 10^{-6}/°C	Pisanova *et al* [11]
Transverse CTE, α_t	18 x 10^{-6}/°C	Pisanova *et al* [11]
Embedded length, l_e	35-50 μm	Master's Thesis Chirag Kareliya [1]

Table 4.4: Mechanical and physical properties of IM7 carbon fiber

The adhesional pressure or and hence, the work of adhesion at the carbon fiber-epoxy interface for the two epoxy systems before and after boiling water degradation are shown in Table 4.6. The experimental results of interfacial shear stress (IFSS) obtained by previous research in our group from the microbond test show that the values of IFSS were lower than the adhesional pressure values obtained here. This is in accordance with the findings by Scheer and Nairn [4]. However, the adhesional

Property	**6F TGMDA**	**DDS TGMDA**	**Source**
External radius of specimen, R_m	20 μm	20 μm	MS Thesis Chirag Kareliya [1]
Tensile modulus, E_m	2.89 GPa	2.71 GPa	Nanoindentation
Poisson's ratio, ν_m	0.3	0.3	Hinkley [7]
Shear modulus, G_m	1.11 GPa	1.04 GPa	$E_m = 2G_m(1+\nu)$
CTE, α_m	35.89 x 10^{-6}/°C	41.23 x 10^{-6}	CGS

Table 4.5: Mechanical and physical properties of the Matrix Systems

Matrix	**Degradation**	**Adhesional Pressure (MPa)**	**Work of Adhesion (mJ/m^2)**
6F TGMDA	As received	135.48±2.42	81.11±0.77
DDS TGMDA	As received	138.47±3.38	82.07±1.08
6F TGMDA	BWD for 24 hrs	134.88±2.97	80.92±0.95
DDS TGMDA	BWD for 24 hrs	137.62±3.61	81.80±1.15

Table 4.6: Adhesional pressure and work of adhesion for 6F TGMDA and DDS TGMDA-carbon fiber composite systems before and after boiling water degradation

pressure at the fiber matrix interface for the two epoxy systems did not differ by much and boiling water degradation also did not have significant effect on it. The work of adhesion, which can be physically interpreted as the work required per unit interfacial area to debond the fiber and matrix interface were in the same order of magnitude as obtained by Pisanova *et al.* [11] for epoxy resin-glass fiber systems. But for the fluorinated and non-fluorinated epoxies, the work of adhesion showed almost similar results.

4.1.4 Fourier Transform Infra-red Spectroscopy

Fourier transform infra-red spectroscopy (FTIR) was done to further understand the effect of incorporating fluorine into the TGMDA base resin. FTIR spectrum for the cured epoxies 6F TGMDA and DDS cured TGMDA are shown in Figure 4.12.

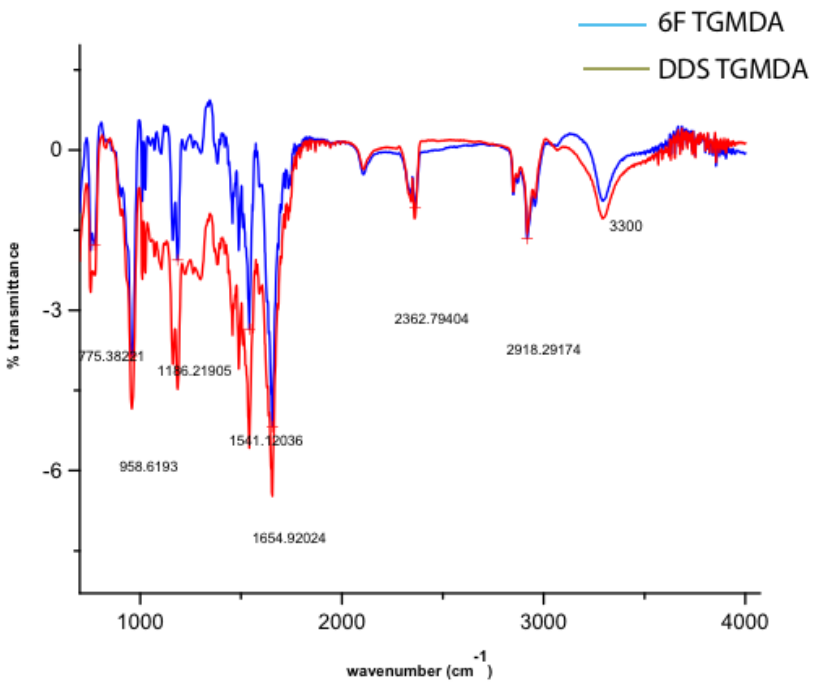

Figure 4.12: Fourier transform infra-red spectra for 6F TGMDA and DDS TGMDA

The two spectra look almost similar and seem to overlap each other. This is

because the peaks caused by the C-F bonds in the fluorinated resin fall within the range of 1000-1300 cm^{-1}. These peaks are masked by the ether peaks (R-O-R) which are formed after curing of the epoxy. Hence, a better approach to understand the chemical differences in the two epoxies responsible for the difference in adhesion, would be Raman spectroscopy. The interpretation of the peak positions in the FTIR spectra is given in Table 4.7.

Peak Position (cm^{-1})	**Characterization**
2918.29 and 3030	C-H stretching vibration of benzene ring
2362.79	Atmospheric carbon dioxide peak
1654.92 and 1541	C=C stretching vibration
1186.21	C-O stretching peak of ether formed after curing
3300	O-H peaks

Table 4.7: Interpretation of peak positions in FTIR spectra for 6F TGMDA and DDS TGMDA

CHAPTER 5

CONCLUSIONS AND FUTURE WORK

The results obtained in this study establish the compatibility of fluorinated resin 6F TGMDA as a matrix material in carbon fiber reinforced composites. This is evident from the adhesional pressure values which are comparable to other carbon fiber-epoxy composite systems [11]. Also, the adhesional pressure or normal stress at the interface was seen to be higher than the interfacial shear stress (IFSS) found in earlier studies [1]. This is in accordance with the findings of Scheer and Nairn [4]. Hence, the criteria for interfacial failure should be adhesional pressure, which is a more accurate way to characterize the interface rather than average IFSS. In the process of determining the interfacial adhesion, the mechanical and physical properties of the fiber and epoxy were determined. The relaxation modulus of the fluorinated and non-fluorinated epoxy were determined using Nano-indentation technique and the Coefficient of Thermal Expansion (CTE) was calculated from Coherent Gradient Sensing. Using the values of these parameters for the as received and degraded epoxy, the adhesional pressure was estimated.

The principal focus of this study was to determine the effect of fluorination of the TGMDA based epoxy, on interfacial adhesion. This did not prove to be a significant success since the adhesional pressure at the interface was found to be similar for both the fluorinated and non-fluorinated epoxy systems. Also, moisture degradation did not change the values of these parameters significantly. The two significant effects of fluorination of the epoxy can be listed as increase in relaxation modulus as compared to the non-fluorinated epoxy and a lower value of CTE, which implies that the

thermal stresses at the interface will be lower for the fluorinated epoxy. However, the combined effect of these parameters did not affect the interfacial normal stress significantly. The adhesional pressure for 6F TGMDA-carbon fiber interface was found to be 135.48±2.42 MPa compared to 138.47±3.38 MPa for the DDS TGMDA-carbon fiber interface. The marginal variation in these values maybe assigned to experimental error. The fact that the adhesional pressure does not show significant decrease upon fluorination of the epoxy system is an advantage. The hydrophobicity of fluorine can be utilized to manufacture environmentally resistant composites while keeping the level of interfacial adhesion the same as in the case of conventional epoxy system, DDS cured TGMDA. On boiling water degradation for 24 hours, the reduction in adhesional pressure was minimal in both cases: 0.23% for the 6F TGMDA system and 0.32% for the DDS TGMDA system. We can conclude that this analytical approach, though useful for characterizing adhesion for a given fiber-matrix interface, may not be adequate to monitor changes in adhesion over a degradation process since, it does not directly measure adhesion. Rather it measures adhesion as a function of the change in properties of the fiber and matrix involved. Another source of inaccuracy in this analysis was measuring the debond force in the microbond experiment. The debond force used in this analysis was an average of the maximum force reached in microbond experiments for the respective fiber-matrix systems. However, a more accurate measurement of the debond force would be to monitor crack propagation at the interface as a function of applied force. The force should be plotted as a function of crack length and then, extrapolated to zero crack length to obtain the accurate debond force.

In order to develop a more realistic approach to characterize interfacial adhesion and understand load transfer mechanisms at the interface, some methods can be employed subsequently:

- The tensile testing of the microcomposites can be carried out under an optical microscope and hence the crack initiation and propogation can be monitored in situ. An energy release rate model based on fracture mechanics approach, which takes into account both friction at fiber-matrix interface and residual thermal stresses, could be used to estimate the local failure criterion for determining fiber-matrix interface strength. [39]

- Raman spectroscopy can be used to map the strain in the fiber as the matrix is loaded in tension. This can be used to obtain Interfacial Shear Stress henceforth to quantify adhesion at the interface. [52]

- The microbond experimental technique can be modified by introducing a pre-existing crack length along the fiber-matrix interface. This can be achieved by coating part of the carbon fiber by a coating agent and depositing the epoxy micro-droplet partially on the coated fiber and partially on the uncoated length of the fiber. This would form a novel microfracture experiment which would potentially characterize the fiber-matrix interface very accurately.

- The fluorinated epoxy, by its very nature is hydrophobic and hence is expected to adhere to the carbon fiber surface less than the non-fluorinated epoxy, DDS TGMDA. Surface treatment of the carbon fibers may cause improvement in the interfacial adhesion [10, 52].

BIBLIOGRAPHY

[1] C. H. Kareliya, "Interfacial micromechanics and effect of moisture on fluorinated epoxy carbon fiber composites," *Masters' Thesis, Oklahoma State University*, 2009.

[2] M. Hanson, "Production of boeing 787 dreamliners," *Boeing News*.

[3] "http://en.wikipedia.org/wiki/haltejas," December 2009.

[4] R. J. Scheer and J. A. Nairn, "A comparison of several fracture mechanics methods for measuring interfacial toughness with microbond tests," *Journal of Adhesion*, vol. 53, no. 1-2, pp. 45–68, 1995. Times Cited: 42.

[5] P. Mallick, "Composites engineering handbook, issue 14702," *Materials Engineering*, vol. 11, p. 121, 1997.

[6] R. B. Durairaj, "Resorcinol: chemistry, technology and applications," p. 748, 2005.

[7] J. Hinkley, "Private communication," 2007.

[8] J. A. Barrie, P. S. Sagoo, and P. Johncock, "The sorption and diffusion of water in halogen-containing epoxy-resins," *Polymer*, vol. 26, no. 8, pp. 1167–1171, 1985. Times Cited: 16.

[9] H. S. Chemicals, "Epon 862/epikure 3234 technical data sheet inc," 2008.

[10] K. K. C. Ho, G. Kalinka, M. Q. Tran, N. V. Polyakova, and A. Bismarck, "Fluorinated carbon fibres and their suitability as reinforcement for fluoropolymers,"

Composites Science and Technology, vol. 67, pp. 2699–2706, 2007. Times Cited: 10.

[11] E. Pisanova, S. Zhandarov, and E. Mader, "How can adhesion be determined from micromechanical tests?," *Composites Part a-Applied Science and Manufacturing*, vol. 32, no. 3-4, pp. 425–434, 2001. Times Cited: 24 6th International Conference on Interfacial Phenomena in Composite Materials SEP 08-10, 1999 Steglitz Int, Berlin, Germany.

[12] M. R. Piggott, "A new model for interface failure in fibre-reinforced polymers," *Composites Science and Technology*, vol. 55, no. 3, pp. 269 – 276, 1995.

[13] Z. Dai, F. Shi, B. Zhang, M. Li, and Z. Zhang, "Effect of sizing on carbon fiber surface properties and fibers/epoxy interfacial adhesion," *Applied Surface Science*, vol. 257, pp. 6980–6985, MAY 15 2011.

[14] Z. Xu, L. Chen, Y. Huang, J. Li, X. Wu, X. Li, and Y. Jiao, "Wettability of carbon fibers modified by acrylic acid and interface properties of carbon fiber/epoxy," *European Polymer Journal*, vol. 44, pp. 494–503, FEB 2008.

[15] H. Wagner, H. Gallis, and E. Wiesel, "Study of the Interface In Kevlar 49-Epoxy Composites by means of Microbond and Fragmentation Tests-Effects of Materials and Testing Variables," *Journal of Materials Science*, vol. 28, pp. 2238–2244, APR 15 1993.

[16] M. Nardin, E. Asloun, and J. Schultz, "Acid-base interactions at carbon-fiber peek interfaces," *Surface and Interface Analysis*, vol. 17, pp. 485–488, JUN 1991.

[17] Z. Q. Taa, S. Y. Yang, Z. Y. Ge, J. S. Chen, and L. Fan, "Synthesis and properties of novel fluorinated epoxy resins based on 1,1-bis(4-glycidylesterphenyl)1-(3'-trifluoromethylphenyl)-2,2,2-trifluo roethane," *European Polymer Journal*, vol. 43, no. 2, pp. 550–560, 2007. Times Cited: 0.

[18] S. Sasaki and K. Nakamura, "Syntheses and properties of cured epoxy-resins containing the perfluorobutenyloxy group .1. epoxy-resin cured with perfluorobutenyloxyphthalic anhydride," *Journal of Polymer Science Part a-Polymer Chemistry*, vol. 22, no. 3, pp. 831–840, 1984. Times Cited: 17.

[19] D. Hayward, E. Hollins, P. Johncock, I. McEwan, R. A. Pethrick, and E. A. Pollock, "The cure and diffusion of water in halogen containing epoxy/amine thermosets," *Polymer*, vol. 38, no. 5, pp. 1151–1168, 1997. Times Cited: 20.

[20] Y. B. Chong and H. Ohara, "Modification of carbon-fiber surfaces by direct fluorination," *Journal of Fluorine Chemistry*, vol. 57, no. 1-3, pp. 169–175, 1992. Times Cited: 24.

[21] M. Pitkethly and J. Doble, "Characterizing the fibre/matrix interface of carbon fibre-reinforced composites using a single fibre pull-out test," *Composites*, vol. 21, no. 5, pp. 389 – 395, 1990.

[22] A. Domnanovich, H. Peterlik, and K. Kromp, "Determination of interface parameters for carbon/carbon composites by the fibre-bundle pull-out test," *Composites Science and Technology*, vol. 56, no. 9, pp. 1017 – 1029, 1996.

[23] S.-Y. Fu, C.-Y. Yue, X. Hu, and Y.-W. Mai, "Analyses of the micromechanics of stress transfer in single- and multi-fiber pull-out tests," *Composites Science and Technology*, vol. 60, no. 4, pp. 569 – 579, 2000.

[24] C. DiFrancia, T. C. Ward, and R. O. Claus, "The single-fibre pull-out test. 2: Quantitative evaluation of an uncatalysed tgddm/dds epoxy cure study," *Composites Part A: Applied Science and Manufacturing*, vol. 27, no. 8, pp. 613 – 624, 1996.

[25] Y. Qiu and P. Schwartz, "Single-fiber pull-out from a microcomposite test," *Composites Science and Technology*, vol. 48, no. 1-4, pp. 5 – 10, 1993. Special Issue Microphenomena in Advanced Composites.

[26] C. Y. Yue, H. C. Looi, and M. Y. Quek, "Assessment of fibre-matrix adhesion and interfacial properties using the pull-out test," *International Journal of Adhesion and Adhesives*, vol. 15, no. 2, pp. 73 – 80, 1995.

[27] S. Deng, L. Ye, Y.-W. Mai, and H.-Y. Liu, "Evaluation of fibre tensile strength and fibre/matrix adhesion using single fibre fragmentation tests," *Composites Part A: Applied Science and Manufacturing*, vol. 29, no. 4, pp. 423 – 434, 1998.

[28] C. Schutte, W. McDonough, M. Shioya, M. McAuliffe, and M. Greenwood, "The use of a single-fibre fragmentation test to study environmental durability of interfaces/interphases between dgeba/mpda epoxy and glass fibre: the effect of moisture," *Composites*, vol. 25, no. 7, pp. 617 – 624, 1994. Third International Conference on Interfacial Phenomena in Composite Materials.

[29] T. J. Copponnex, "Analysis and evaluation of the single-fibre fragmentation test," *Composites Science and Technology*, vol. 56, no. 8, pp. 893 – 909, 1996.

[30] M. J. Greenfield, A. Pedicini, and L. S. Penn, "Development of a single fiber fragmentation test for high strain rates," *International Journal of Adhesion and Adhesives*, vol. 20, no. 5, pp. 403 – 407, 2000.

[31] J. Varna, R. Joffe, and L. A. Berglund, "Interfacial toughness evaluation from the single-fiber fragmentation test," *Composites Science and Technology*, vol. 56, no. 9, pp. 1105 – 1109, 1996.

[32] A. Awal, G. Cescutti, S. Ghosh, and J. Mssig, "Interfacial studies of natural fibre/polypropylene composites using single fibre fragmentation test (sfft)," *Com-*

posites Part A: Applied Science and Manufacturing, vol. 42, no. 1, pp. 50 – 56, 2011.

[33] B. Miller, P. Muri, and L. Rebenfeld, "A microbond method for determination of the shear strength of a fiber/resin interface," *Composites Science and Technology*, vol. 28, no. 1, pp. 17 – 32, 1987.

[34] U. Gaur and B. Miller, "Microbond method for determination of the shear strength of a fiber/resin interface: Evaluation of experimental parameters," *Composites Science and Technology*, vol. 34, no. 1, pp. 35 – 51, 1989.

[35] P. J. Herrera-Franco, V. Rao, L. T. Drzal, and M. Y. Chiang, "Bond strength measurement in composites–analysis of experimental techniques," *Composites Engineering*, vol. 2, no. 1, pp. 31 – 45, 1992.

[36] D. A. Biro, G. Pleizier, and Y. Deslandes, "Application of the microbond technique: Effects of hygrothermal exposure on carbon-fiber/epoxy interfaces," *Composites Science and Technology*, vol. 46, no. 3, pp. 293 – 301, 1993.

[37] T. Schller, U. Bahr, W. Beckert, and B. Lauke, "Fracture mechanics analysis of the microbond test," *Composites Part A: Applied Science and Manufacturing*, vol. 29, no. 9-10, pp. 1083 – 1089, 1998.

[38] H. Kessler, T. Schller, W. Beckert, and B. Lauke, "A fracture-mechanics model of the microbond test with interface friction," *Composites Science and Technology*, vol. 59, no. 15, pp. 2231 – 2242, 1999.

[39] C.-H. Liu and J. A. Nairn, "Analytical and experimental methods for a fracture mechanics interpretation of the microbond test including the effects of friction and thermal stresses," *International Journal of Adhesion and Adhesives*, vol. 19, no. 1, pp. 59 – 70, 1999.

[40] J. A. Nairn, "Fracture mechanics of composites with residual stresses, imperfect interfaces, and traction-loaded cracks," *Composites Science and Technology*, vol. 61, no. 15, pp. 2159 – 2167, 2001.

[41] J. T. Ash, W. M. Cross, D. Svalstad, J. J. Kellar, and L. Kjerengtroen, "Finite element evaluation of the microbond test: meniscus effect, interphase region, and vise angle," *Composites Science and Technology*, vol. 63, no. 5, pp. 641 – 651, 2003.

[42] M. Nishikawa, T. Okabe, K. Hemmi, and N. Takeda, "Micromechanical modeling of the microbond test to quantify the interfacial properties of fiber-reinforced composites," *International Journal of Solids and Structures*, vol. 45, no. 14-15, pp. 4098 – 4113, 2008.

[43] P. Herrera-Franco and L. Drzal, "Comparison of methods for the measurement of fibre/matrix adhesion in composites," *Composites*, vol. 23, no. 1, pp. 2 – 27, 1992.

[44] L. T. Drzal, P. J. Herrera-Franco, and H. Ho, "Fiber-matrix interface tests," in *Comprehensive Composite Materials* (A. Kelly and C. Zweben, eds.), pp. 71 – 111, Oxford: Pergamon, 2000.

[45] S. Zhandarov, Y. Gorbatkina, and E. Mder, "Adhesional pressure as a criterion for interfacial failure in fibrous microcomposites and its determination using a microbond test," *Composites Science and Technology*, vol. 66, no. 15, pp. 2610 – 2628, 2006.

[46] H. Corporation, "Hextow im7 carbon fibers," *HexTow IM7 Product Sheet*, 2009.

[47] G. Huang and H. B. Lu, "Measurement of young's relaxation modulus using nanoindentation," *Mechanics of Time-Dependent Materials*, vol. 10, no. 3, pp. 229–243, 2006. Times Cited: 10.

[48] H. V. Tippur and A. J. Rosakis, "Quasi-static and dynamic crack-growth along bimaterial interfaces - a note on crack-tip field-measurements using coherent gradient sensing," *Experimental Mechanics*, vol. 31, no. 3, pp. 243–251, 1991. Times Cited: 77.

[49] A. J. Rosakis, R. P. Singh, Y. Tsuji, E. Kolawa, and N. R. Moore, "Full field measurements of curvature using coherent gradient sensing: application to thin film characterization," *Thin Solid Films*, vol. 325, no. 1-2, pp. 42–54, 1998. Times Cited: 32.

[50] N. J. J. C. M. M. Miller, Sandi; Leventis, "Clay nanocomposite/aerogel sandwich structures for cryotanks," *NASA Technical Reports Server*, 2006.

[51] H. Miyagawa, C. Sato, T. Mase, E. Drown, L. Drzal, and K. Ikegami, "Transverse elastic modulus of carbon fibers measured by Raman spectroscopy," *Materials Science and Engineering A-Structural Materials Properties Microstructure And Processing*, vol. 412, pp. 88–92, DEC 5 2005.

[52] M. A. Montes-Morn and R. J. Young, "Raman spectroscopy study of high-modulus carbon fibres: effect of plasma-treatment on the interfacial properties of single-fibre-epoxy composites: Part ii: Characterisation of the fibre-matrix interface," *Carbon*, vol. 40, no. 6, pp. 857 – 875, 2002.

APPENDIX A

Auxiliary Constants for Adhesional Pressure Algorithm

The auxiliary constants used in the algorithm to determine the adhesional pressure depend on the geometry of the microbond samples and the mechanical and physical properties of the epoxy. They are defined as follows:

$$A_0 = \frac{V_m(1-\nu_t)}{V_f E_t} + \frac{1-\nu_m}{E_m} + \frac{1+\nu_m}{V_f E_m}$$

$$A_1 = \left(\frac{1-\nu_t}{E_t} - \frac{1-\nu_m}{E_m}\right)(1+\nu_m)\left(1+\frac{2lnV_f}{V_m}\right) + \frac{2(1-\nu_m)}{V_m E_m}$$

$$A_2 = \frac{1-\nu_t}{E_t} - \frac{1-\nu_m}{E_m}$$

$$A_3 = -\left(\frac{\nu_A}{E_A} + \frac{V_f \nu_m}{V_m E_m}\right)$$

$$A_4 = \frac{\nu_m}{V_m E_m}$$

$$A_5 = \alpha_t - \alpha_m$$

$$C_{33} = \frac{1}{2}\left(\frac{1}{E_A} + \frac{V_f}{V_m E_m}\right) - \frac{V_m A_3^2}{V_f A_0}$$

$$C_{35} = \frac{1}{16}\left(A_3\left[(1+\nu_m)\left(1+\frac{2lnV_f}{V_m}\right) - \frac{V_m A_1}{V_f A_0}\right] - 2A_4\right)$$

$$C_{55} = \frac{1}{256}\left(\frac{1-\nu_t}{E_t}\left[\frac{5+2\nu_t}{3}+\nu_m(2+\nu_m)\right]+\frac{4A_2(1+\nu_m)^2 lnV_f}{V_m}\left(1+\frac{lnV_f}{V_m}\right)-\frac{V_m A_1^2}{V_f A_0}+\frac{1-\nu_m}{E_m}\right.$$
$$\left.\times\left[\frac{V_m^2(1+\nu_m)(5+3\nu_m)-3V_m(1+\nu_m)(3+\nu_m)+6(5+3\nu_m)}{3V_f V_m}+\frac{8(1+\nu_m)lnV_f}{V_m^2}\right]\right)$$

$$C_{44} = \frac{1}{16}\left[\frac{1}{G_A}-\frac{1}{G_m}\left(1+\frac{2}{V_m}+\frac{2lnV_f}{V_m^2}\right)\right]$$

$$C_{13} = -\frac{1}{2V_m E_m}-\frac{V_m A_3 A_4}{V_f A_0}$$

$$C_{11} = \frac{1}{2V_f V_m E_m}-\frac{V_m A_4^2}{V_f A_0}$$

$$D_3 = -\frac{V_m A_3}{V_f A_0}(\alpha_t-\alpha_m)+\frac{1}{2}(\alpha_A-\alpha_m)$$

$$p = \frac{2C_{35}-C_{44}}{C_{55}}$$

$$q = \frac{C_{33}}{C_{55}}$$

$$D = p^2-4q$$

VITA

Suman Dasgupta

Candidate for the Degree of

Master of Science

Thesis: CHARACTERIZATION OF ADHESION AT CARBON FIBER-FLUORINATED EPOXY INTERFACE AND EFFECT OF ENVIRONMENTAL DEGRADATION

Major Field: Mechanical and Aerospace Engineering

Biographical:

Personal Data: Born in Kolkata, West Bengal, India on January 15, 1987.

Education:

Received the B.S. degree from Jadavpur University, Kolkata, West Bengal, India, 2009, in Mechanical Engineering

Completed the requirements for the degree of Master of Science with a major in Mechanical and Aerospace Engineering Oklahoma State University in June 2011.

Experience:

Worked as a Graduate Research Assistant at the Mechanics of Advanced Materials Laboratory headed by Dr. Raman P. Singh in the area of polymer reinforced composites.

Name: Suman Dasgupta Date of Degree: June, 2011

Institution: Oklahoma State University Location: Stillwater, Oklahoma

Title of Study: CHARACTERIZATION OF ADHESION AT CARBON FIBER-FLUORINATED EPOXY INTERFACE AND EFFECT OF ENVIRONMENTAL DEGRADATION

Pages in Study: 51 Candidate for the Degree of Master of Science

Major Field: Mechanical and Aerospace Engineering

Carbon fiber reinforced polymers are excellent candidates for aerospace, automobile and other mobile applications due to their high specific strength and modulus. The most prominent aerospace application of carbon fiber composites in recent times is the Boeing 787 Dreamliner, which is the world's first major commercial airliner to extensively use composite materials. The critical issue, which needs to be addressed hereby, is long-term safety. Hence, long-term durability of composite materials in such applications becomes a point of concern. Conventional polymer matrices, such as thermosetting resins, which are used as matrix material in carbon fiber composites, are susceptible to degradation in the form of chemical corrosion, UV degradation and moisture, in severe environmental conditions. Fluorinated polymers offer a viable alternative as matrix material, due to their reduced susceptibility to environmental degradation. The epoxy system used in this study is fluorinated Tetra-glycidyl methylene di-aniline (6F-TGMDA), which was developed by polymer scientists at NASA Langley Research Center. The hydrophobic nature of this epoxy makes it a potential matrix material in aerospace applications. However, its compatibility in carbon fiber-reinforced composites remains to be investigated. This study aims to characterize the interfacial properties in carbon fiber reinforced fluorinated epoxy composites. Typical interfacial characterization parameters, like interfacial shear strength, estimated from the microbond test, proved to be inadequate in accurately estimating adhesion since it assumes a uniform distribution of stresses along the embedded fiber length. Also, it does not account for any residual stresses present at the interface, which might arise due to thermal expansion differences and Poisson's ratio differences of the fiber and matrix. Hence, an analytical approach, which calculates adhesion pressure at the interface, was adopted. This required determination of the unknown mechanical and physical properties of the resin, the relaxation modulus (determined using nano-indentation) and coefficient of thermal expansion (determined using coherent gradient sensing). The adhesional pressure for 6F TGMDA-carbon fiber interface was found to be 135.15 MPa compared to 138.27 MPa for the Diamino diphenyl sulphone (DDS) cured TGMDA-carbon fiber interface. The fact that the adhesional pressure does not show significant decrease upon fluorination of the epoxy system is an advantage. The hydrophobicity of fluorine can be utilized to manufacture environmentally resistant composites while keeping the level of interfacial adhesion the same as in the case of conventional epoxy system, DDS cured TGMDA.

ADVISOR'S APPROVAL: _____